*J Physiol* (2003), **549.2**, *pp.* 439–452
DOI: 10.1113/jphysiol.2002.034413

www.jphysiol.org

Journal of Physiology

# Extracellular vestibule determinants of $Ca^{2+}$ influx in $Ca^{2+}$-permeable AMPA receptor channels

Claudia Jatzke, Matthew Hernandez and Lonnie P. Wollmuth

*Department of Neurobiology and Behavior, State University of New York at Stony Brook, Stony Brook, NY 11794-5230, USA*

**At certain synapses in the brain, $Ca^{2+}$-permeable AMPA receptor (AMPAR) channels represent an important pathway for synaptically controlled $Ca^{2+}$ entry. However, the molecular determinants of this $Ca^{2+}$ influx are poorly defined. In NMDA receptor (NMDAR) channels, where the influx is much greater, the extracellular vestibule, specifically the M3 segment and regions C-terminal to it in the NR1 subunit, contains elements critical to their high $Ca^{2+}$ influx under physiological conditions. We therefore investigated the contribution of homologous positions in AMPAR as well as kainate receptor (KAR) subunits to the process of $Ca^{2+}$ influx. Substitutions of a conserved asparagine (N) in M3 of AMPAR GluR-B(Q) channels strongly attenuated $Ca^{2+}$ permeability measured using reversal potentials under biionic conditions and fractional $Ca^{2+}$ currents recorded under physiological conditions. Hence, as in NMDAR channels, the conserved N makes a significant contribution to $Ca^{2+}$ influx in AMPAR channels. In addition, C-terminal to M3, substitutions of negatively (glutamate, E) or positively (arginine, R) charged residues also altered $Ca^{2+}$ influx. However, in contrast to charged residues occupying homologous positions in NMDAR channels, these effects were about equal and opposite suggesting that this ER in AMPARs does not contribute significantly to the mechanism of $Ca^{2+}$ influx. Opposite charge substitutions of two negative residues C-terminal to M3 in KAR GluR-6(Q) subunits had no effect on $Ca^{2+}$ permeability. We conclude that the different contribution of residues C-terminal to M3 to $Ca^{2+}$ permeation in NMDAR and non-NMDAR channels reflects a different positioning of these residues relative to the tip of the M2 loop.**

(Received 13 October 2002; accepted after revision 18 March 2003; first published online 11 April 2003)
**Corresponding author** L. P. Wollmuth: Department of Neurobiology and Behavior, State University of New York at Stony Brook, Stony Brook, NY 11794-5230, USA. Email: lwollmuth@notes1.cc.sunysb.edu

Glutamate receptor (GluR) channels, when activated by glutamate, represent a pathway for $Ca^{2+}$ entry into a cell (Dingledine *et al.* 1999). At most synapses, the major mechanism mediating this $Ca^{2+}$ entry is the *N*-methyl-D-aspartate receptor (NMDAR) subtype. However, at certain synapses, typically those associated with interneurons, α-amino-3-hydroxy-5-methyl-4-isoxazole-propionate receptor (AMPAR) channels can also be $Ca^{2+}$ permeable (Burnashev, 1996). Indeed, the $Ca^{2+}$ influx mediated by $Ca^{2+}$-permeable AMPAR channels has physiological significance, underlying synaptic modulation (Gu *et al.* 1996; Mahanty & Sah, 1998; Liu & Cull-Candy, 2000) as well as functional relationships between glial cells and synapses (Iino *et al.* 2001). Despite this importance, determinants of $Ca^{2+}$ influx in $Ca^{2+}$-permeable AMPAR and kainate receptor (KAR) channels remain poorly defined.

In GluR channels, $Ca^{2+}$ permeability as well as channel block and single channel conductance are strongly influenced by the amino acid occupying a functionally critical position in the M2 loop, the Q/R site in non-NMDARs and the N site (or N + 1 site) in NMDARs (Dingledine *et al.* 1999). RNA editing of the Q/R site in the AMPAR GluR-B (or GluR2) or the KAR GluR-5 and -6 subunits results in a polar glutamine (Q) being replaced by a positively charged arginine (R) in the mature protein (Seeburg *et al.* 1998). Channels containing the edited or R-form of these subunits are essentially $Ca^{2+}$-impermeable (Burnashev *et al.* 1995) with homomeric R-forms of KAR channels even permeable to $Cl^-$ (Burnashev *et al.* 1996). Hence, the Q/R site, specifically in its edited form, is critical to defining $Ca^{2+}$ permeability. Still, the positively charged arginine can have indirect actions on permeating ions. Accordingly, its effect on $Ca^{2+}$ influx does not indicate that glutamine occupying the Q/R site defines the $Ca^{2+}$ permeability properties of channels containing only non- or unedited subunits. Consistent with this idea, the Q/R site is positioned external to the channel's narrow constriction (Kuner *et al.* 2001), suggesting that the action of the arginine is mainly electrostatic. Hence, other elements in the pore may also contribute to the process of $Ca^{2+}$ influx in $Ca^{2+}$-permeable AMPAR channels. Identifying such elements will help to clarify the mechanism of $Ca^{2+}$ influx in AMPAR channels and will be

useful in the development of mutant mice to study its functional significance.

In NMDAR channels, the extracellular vestibule contains key determinants of their high $Ca^{2+}$ influx (Watanabe *et al.* 2002). These determinants, associated with the NR1 subunit, include DRPEER, a highly charged motif located C-terminal to the M3 segment as well as a highly conserved asparagine (N632) within the M3 SYTANLAAF motif (see Fig. 1). Some of these domains, such as the conserved N, are present in non-NMDAR subunits. On the other hand, most of DRPEER is unique to NR1. DR, however, is conserved in terms of charge, being represented by a negatively charged glutamate (E) and an arginine (R) in non-NMDAR subunits. Further, within regions homologous to DRPEER, KAR subunits possess not only ER but also an additional negative charge at position 634 (E634). It is unclear how these externally located domains contribute to the process of $Ca^{2+}$ influx in non-NMDAR, especially given that the magnitude of this influx is much lower than that in NMDAR channels.

In the present study, we investigated the contribution of these homologous elements in $Ca^{2+}$-permeable non-NMDAR channels to $Ca^{2+}$ influx (Fig. 1). We find that the conserved N in M3 in AMPAR channels makes a significant contribution to this process. On the other hand, charged residues located C-terminal to M3 make either minor (AMPAR) or no (KAR) contribution in contrast to those in NMDAR. We conclude that this difference between the GluR subtypes reflects a structural difference between them, possibly a much more external location of these positions in non-NMDAR subunits relative to the tip of the M2 loop.

## METHODS

### Molecular biology

All experiments were performed with previously described expression constructs for wild type NMDAR, AMPAR and KAR subunits (see Jatzke *et al.* 2002 for references). The KAR subunit, GluR-6, was fully edited within the M1 segment (V,C) (Köhler *et al.* 1993). AMPAR subunits were identified following the nomenclature of Seeburg (1993), with the amino acid occupying the Q/R site indicated in parentheses. Point mutations in GluR-A(Q), GluR-B(Q), GluR-B(N) and GluR-6(Q) were generated either by the QuikChange site-directed mutagenesis kit (Stratagene, LaJolla, CA, USA) or by other PCR-based methods using Platinum Pfx DNA polymerase (Invitrogen, Carlsbad, CA, USA) or Pfu poly DNA polymerase (Stratagene). Positive clones were subcloned back into the respective wild type clone present in the eukaryotic expression vector pRK. All constructs were sequenced over the entire length of the replaced fragment. All AMPAR subunits were of the flip-splice variant form. Channels were expressed transiently in human embryonic kidney 293 (HEK 293) cells using FuGene 6 (Roche, Indianapolis, IN, USA). A vector for enhanced green fluorescent protein (pEGFP-C1, Clontech, Palo Alto, CA, USA) was co-transfected at a ratio of 1:9. Cells were recorded from 1to 3 days after transfection.

### Electrophysiology

Currents were recorded at room temperature (20–23 °C) using an EPC-9 amplifier with PULSE software (HEKA Elektronik, Lambrecht, Germany), low-pass filtered at 300–500 Hz and digitized at 2 kHz. Pipettes had resistances of 2–4 MΩ when filled with the pipette solution and measured in the $Na^+$ reference solution. External solutions were applied using a piezo-driven double-barrel application system. The open tip response

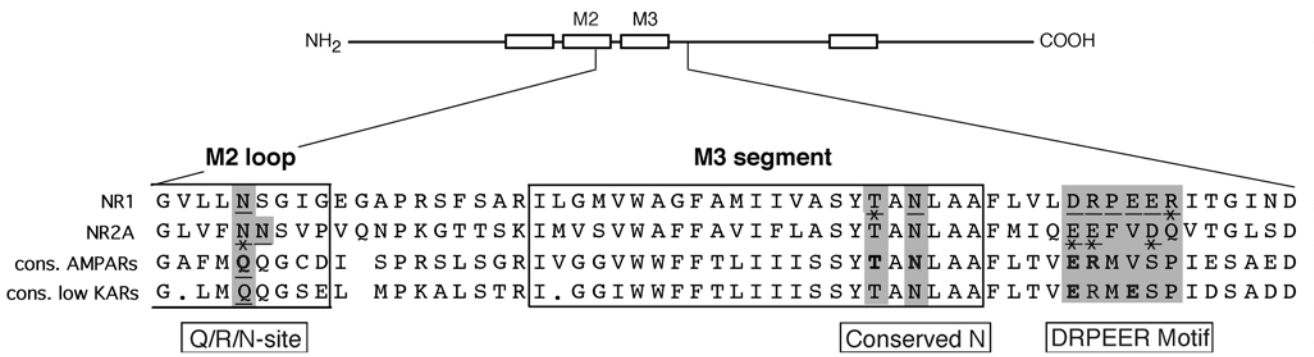


**Figure 1. Sequence alignment of GluR subtypes**

Top, schematic drawing of a GluR subunit with the four hydrophobic domains (M1–M4) shown as open boxes. Bottom, enlarged region (thin lines) comparing the amino acid residues of NR1, NR2A and the consensus sequences of AMPARs (GluR-A, -B, -C, -D) and low-affinity KARs (GluR-5, -6, -7). The dots in the KAR consensus sequence indicate positions that are occupied by non-identical amino acid residues. Open positions represent gaps within the alignment. For NMDAR subunits, residues that have been mutated and tested for effects on $Ca^{2+}$ influx are underlined (Watanabe *et al.* 2002). Mutant channels containing these substitutions either significantly altered $Ca^{2+}$ influx relative to wild type or if not, the underlined marker is crossed out. The shaded areas reflect the homologous positions to them in all subunits. Bold amino acid residues depict positions where site-directed mutagenesis was used to introduce opposite charged or neutral (alanine, A, cysteine, C) residues in non-NMDAR subunits. For the Q/R site, the glutamine Q, of the unedited form of GluR-B was substituted by an asparagine (N). The numbering for the conserved N in the different subunits is: NR1, 632; NR2A, 629; GluR-A, 615; GluR-B, 619; GluR-6, 623.

(10–90 % rise time) of the application system was < 500 μs. For NMDARs, one barrel contained the external solution plus glycine (20 μM), while the other barrel contained the same solution with added glutamate (100 μM). For non-NMDARs, the glutamate concentration was 1 or 3 mM. To minimize desensitization, we included in all external solutions for AMPARs 15 μM cyclothiazide (CTZ; stock solution was 10 mM CTZ in 100 mM NaOH). For KARs, we initially incubated cells for 2–3 min in concanavalin A (0.3 mg $ml^{-1}$) and included concanavalin A in all reference solutions. Unless otherwise stated, all chemicals were obtained from Sigma (St Louis, MO, USA) or J. T. Baker (Phillipsburg, NJ, USA).

### Experimental protocols

**Fractional $Ca^{2+}$ currents.** Fura-2 (1 mM) was loaded into cells via the patch pipette to measure the fraction of the total current carried by $Ca^{2+}$ (see Neher, 1995). Briefly, cells were illuminated alternatively at 360 and 380 nm (2–10 Hz) by a polychromatic illumination system, with fluorescence signals measured using a photodiode (T.I.L.L. Photonics, München, Germany). Fractional $Ca^{2+}$ currents ($P_f$) were quantified using the relationship, $P_f$ (%) = $100Q_{Ca}/Q_T$, where $Q_{Ca}$ and $Q_T$ are the charge carried by $Ca^{2+}$ and the total charge, respectively, during a defined time interval. $Q_T$ was derived from the current integral. $Q_{Ca}$ was derived from the relationship, $Q_{Ca} = \Delta F_{380}/f_{max}$, where $\Delta F_{380}$ is the change in the fluorescence signal with 380 nm excitation and $f_{max}$ is the proportionality constant between the charge carried by inward $Ca^{2+}$ and $\Delta F_{380}$. $\Delta F_{380}$ was normalized to the fluorescence of beads (4.5 μm diameter fluoresbrite BB beads, Polysciences, Inc., Warrington, PA, USA; lot no. 481613) and expressed in 'bead units' (BU).

In measuring fractional $Ca^{2+}$ currents, our intracellular solution consisted of (mM): 140 KCl, 10 Hepes, 1 $K_5$ fura-2, pH 7.2 (KOH). The external solution consisted of (mM): 140 NaCl and 10 Hepes, pH 7.2 (NaOH) and added $CaCl_2$ (1.8 or 20 mM). Fura-2 was obtained from Molecular Probes (Eugene, OR, USA).

**$Ca^{2+}$ permeability.** We used two different approaches to quantify $Ca^{2+}$ permeability relative to $Na^+$ ($P_{Ca}/P_{Na}$). The first approach was based on measuring changes in the reversal potential, $\Delta E_{rev}$, for glutamate-activated currents on replacing $Na^+$ in a $Na^+$-based reference solution with $Ca^{2+}$ (e.g. Jatzke *et al.* 2002). The reference solution consisted of (mM): 140 NaCl and 10 Hepes, pH 7.2 (NaOH). The high $Ca^{2+}$-containing solution consisted of (mM): 110 $Ca^{2+}$ and 10 trizma base, pH 7.3 (HCl). For 0.5, 1.8 or 10 mM, $Ca^{2+}$ was added to a NMDG-based solution (mM): 140 NMDG and 10 Hepes, pH 7.2 (HCl). The pipette solution consisted of (mM): 140 KCl, 10 BAPTA, 10 Hepes, pH 7.2 (KOH). NMDG shows a weak permeability in non-NMDAR channels. We assumed that this NMDG permeability ($P_{NMDG}/P_{Na}$) was approximately 0.02 in GluR-A(Q) and GluR-B(Q), 0.003 in GluR-B(N) and 0.01 in GluR-6(Q) channels (see Jatzke *et al.* 2002 and references therein). We also assume that the mutations in the extracellular vestibule do not alter $P_{NMDG}/P_{Na}$. In measuring reversal potentials, all potentials have been corrected for junction potentials and are indicated as *E*. $\Delta E_{rev}$ values were converted to $P_{Ca}/P_{Na}$ using the Lewis equation (see eqn (7) in Wollmuth & Sakmann, 1998).

The other approach we used to quantify $P_{Ca}/P_{Na}$ is based on $P_f$ measurements and relates $Ca^{2+}$ permeability to $P_f$ values using Goldman-Hodgkin-Katz (GHK) assumptions. We followed the approach of Jatzke *et al.* 2002 (eqn (1)) where we explicitly defined the intracellular and extracellular monovalent composition and their relative permeabilities. All $P_f$ measurements were quantified relative to the reversal potential.

**Block by internal polyamines.** We used the rectification in the current–voltage relation for $Ca^{2+}$-permeable AMPAR channels as an index of the block by intracellular polyamines. To quantify this rectification, we generated current–voltage relations from −80 to 40 mV in 10 mV increments (see Fig. 2*E*). A fourth-order polynomial was then fitted to the current–voltage relation to verify that the reversal potential was within several millivolts of zero. To derive the rectification ratio, we divided the absolute current at −50 mV by the average current from 10 to 40 mV ($|I_{-50\ mV}|/avg(I_{10-40\ mV})$).

**Gating kinetics.** To determine basic gating characteristics, we recorded currents at −60 mV in outside-out patches isolated from HEK 293 cells in the absence of CTZ. To derive the time constant of desensitization ($\tau_{des}$), we fitted a single exponential to the current decay during a 100 ms glutamate application. The extent of desensitization, represented as a percentage (% des), was derived from the ratio of steady-state ($I_s$) to peak ($I_P$) current amplitudes during the 100 ms application (% des = $100(1 - I_S/I_P)$). To derive the time constant of deactivation ($\tau_{deact}$), we fitted a single exponential to the current decay following a 1 ms glutamate application.

**Glutamate concentration dependence.** The functional concentration–response curve was measured in the whole-cell mode and in the presence of CTZ. Cells were held at −60 mV and solutions containing various concentrations of glutamate (0.01–5 mM) were applied with current amplitudes normalized to that in 5 mM glutamate, plotted as a function of concentration and fitted with the Hill equation $1/(1 + (EC_{50}/[Glu])^{n_H})$ where $EC_{50}$ the concentration to achieve half-maximal response and $n_H$ the Hill coefficient.

### Data analysis

All curve fitting was done using Igor Pro (WaveMetrics, Inc., Lake Oswego, OR, USA). Results are reported as means ± S.E.M. and shown graphically as means ± 2 S.E.M. An analysis of variance was used to test for statistical differences with the Tukey test used for multiple comparisons. Significance was assumed if $P < 0.05$.

## RESULTS

The mechanism of $Ca^{2+}$ influx appears to be comparable across all $Ca^{2+}$-permeable AMPAR channels (e.g. Jatzke *et al.* 2002). As a background for many of our experiments, we therefore typically used the unedited form of GluR-B, where a glutamine occupies the Q/R site (GluR-B(Q)) since other substitutions of the Q/R site already exist for this subunit (e.g. GluR-B(N)). We initially examined the contribution of the conserved asparagine to the process of $Ca^{2+}$ influx in AMPAR channels.

### GluR-B(Q) channels containing substitutions of the conserved N in the M3 segment alter $Ca^{2+}$ permeability

Figure 2*A–C* shows current–voltage relations for cells expressing wild type (B(Q)) or mutant GluR-B(Q) channels containing either cysteine (B(Q)(N619C)) or the positively charged lysine (B(Q)(N619K)) substituted for the conserved asparagine in the M3 segment. (Cells

transfected with the alanine substitution of this position did not yield detectable glutamate-activated currents.) Cells were bathed either in the $Na^+$ reference solution (filled circles) or in solutions where $Na^+$ was replaced by different concentrations of $Ca^{2+}$, 1.8 mM (open diamonds) or 110 mM (open squares). For all channels, currents reversed near −5 mV in the $Na^+$ solution. For wild type when $Na^+$ was replaced by $Ca^{2+}$, the reversal potential was shifted along the axis by 19.2 ± 0.7 mV (mean ± S.E.M.) ($n = 6$) in 110 mM $Ca^{2+}$ and −59.0 ± 0.6 mV ($n = 7$) in 1.8 mM $Ca^{2+}$. For the mutant channels, the reversal potential shifts differed significantly from those in wild type. Indeed, for B(Q)(N619C) and B(Q)(N619K) channels, the shifts were −15.3 ± 2.6 mV ($n = 4$) and −45.5 ± 1.0 mV ($n = 4$), respectively, in 110 mM $Ca^{2+}$ and −84.5 ± 0.8 mV ($n = 3$) and −95.9 ± 0.9 mV ($n = 5$), respectively, in 1.8 mM $Ca^{2+}$.

We used these shifts in reversal potentials to derive average $Ca^{2+}$ permeability ratios ($P_{Ca}/P_{Na}$; Fig. 2*D*). For wild type, $P_{Ca}/P_{Na}$ was essentially concentration independent with an average $P_{Ca}/P_{Na}$ of around 1.72. For both mutant channels,

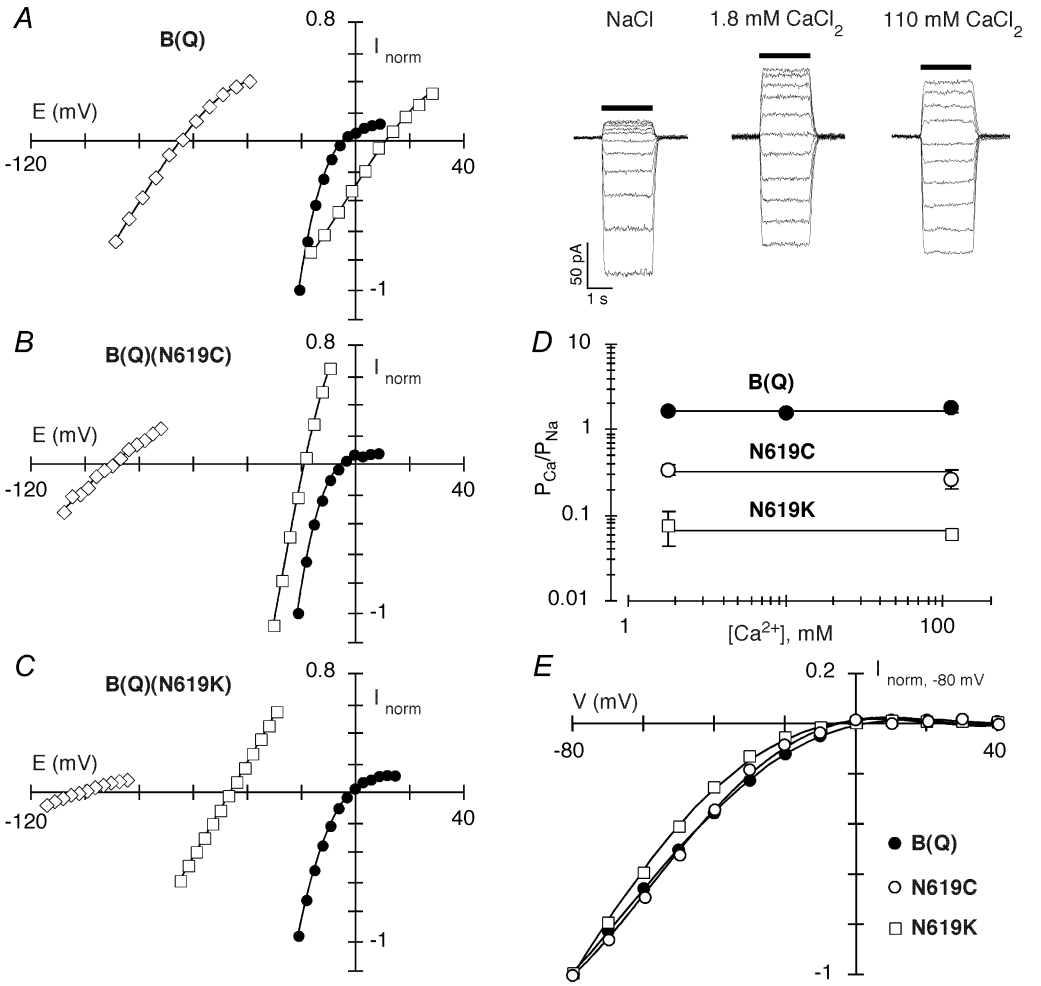


**Figure 2. Effect of substitutions of the conserved N in GluR-B(Q) channels on $Ca^{2+}$ permeability**

*A–C*, average glutamate-activated currents at different membrane potentials, in 2–5 mV increments, in cells expressing GluR-B(Q) (*A*), GluR-B(Q)(N619C) (*B*) or GluR-B(Q)(N619K) (*C*) subunits. The cells were bathed in either 140 mM NaCl (●), 1.8 mM $CaCl_2$, 140 mM NMDG (◇) or 110 mM $CaCl_2$ (□). The NaCl recording is an average of the currents before and after each $CaCl_2$ recording. For comparison, current amplitudes are normalized ($I_{norm}$) to the amplitude at −20 mV in the NaCl solution. *A*, right panel, corresponding whole-cell glutamate-activated currents (glutamate application, horizontal bar, 200 ms) for the GluR-B(Q) current–voltage plot shown in the left panel. All external solutions contained cyclothiazide (CTZ; 15 μM). *D*, average $P_{Ca}/P_{Na}$ (±2 S.E.M.), derived from changes in reversal potentials, such as those shown in *A–C*, for various $Ca^{2+}$ concentrations. The continuous lines are the average $P_{Ca}/P_{Na}$ for all concentrations tested. These average $P_{Ca}/P_{Na}$ values are: 1.72, GluR-B(Q); 0.31, B(Q)(N619C); and 0.07, B(Q)(N619K). A minimum of 4 cells was recorded at each concentration. *E*, current–voltage relationships for cells expressing GluR-B(Q), B(Q)(N619C) or B(N)(N619K) subunits. For comparison, current amplitudes are normalized to that at −80 mV. Cells were bathed in 5 mM $CaCl_2$ and 140 mM NaCl.

**Table 1. Comparison of gating properties of wild type and mutant GluR-B (Q) channels**

| Subunit combination | $\tau_{des}$ (ms) | % des | $\tau_{deact}$ (ms) | $EC_{50}$ ($\mu$M) |
|---|---|---|---|---|
| GluR-B(Q) | 5.8 ± 0.5 (6) | 96 ± 0.8 (7) | 0.6 ± 0.1 (3) | 110 ± 10 |
| B(Q)(N619C) | 5.8 ± 0.6 (3) | 97 ± 0.5 (3) | 0.7 ± 0.1 (3) | 120 ± 20 |

Values shown as means ± S.E.M. (number of recordings). For the $EC_{50}$ measurements, at least three cells were recorded at each concentration. The external solution contained 1.8 mM $CaCl_2$ and 140 mm NaCl. $\tau_{des}$, time constant of desensitization; % des, extent (% des) of desensitization; $\tau_{deact}$, time constant of deactivation.

$P_{Ca}/P_{Na}$ was again essentially concentration independent, but was greatly reduced in magnitude to around 0.31 for B(Q)(N619C) and 0.07 for B(Q)(N619K). Hence, substitutions of the conserved asparagine strongly attenuate $Ca^{2+}$ influx as assayed by reversal potentials.

Substitutions of the conserved N could indirectly affect $Ca^{2+}$ permeation by disrupting pore structure, including that of the M2 loop where the Q/R site is located. To test this idea, we characterized the rectifying current–voltage relation in GluR-B(Q), B(Q)(N619C) and B(Q)(N619K) channels as an index of the block by intracellular polyamines (Bowie & Mayer, 1995; Koh *et al.* 1995). Figure 2*E* shows that the normalized current–voltage relations in these channels are highly comparable. For GluR-B(Q), the rectification ratio (see Methods) was 50 ± 10 ($n$ = 5). For B(Q)(N619C) and B(N)(N619K), the ratios were 39 ± 7 ($n$ = 4) and 62 ± 11 ($n$ = 3), values not significantly different from those in wild type. Since the cysteine substitution (B(Q)(N619C)) is critical to our conclusion, we also compared its gating properties with those of wild type to verify that its effects on $Ca^{2+}$ permeation are not due to changes in gating. As summarized in Table 1, none of the measured parameters including the rate ($\tau_{des}$) and extent (% des) of desensitization, the rate of deactivation ($\tau_{deact}$) and the glutamate concentration for half-maximal activation ($EC_{50}$) were significantly different for B(Q) and B(Q)(N619C) channels. Hence, although we cannot completely rule out alternative functions, this lack of an effect on other channel properties suggests that substitutions of the conserved N are directly affecting $Ca^{2+}$ influx.

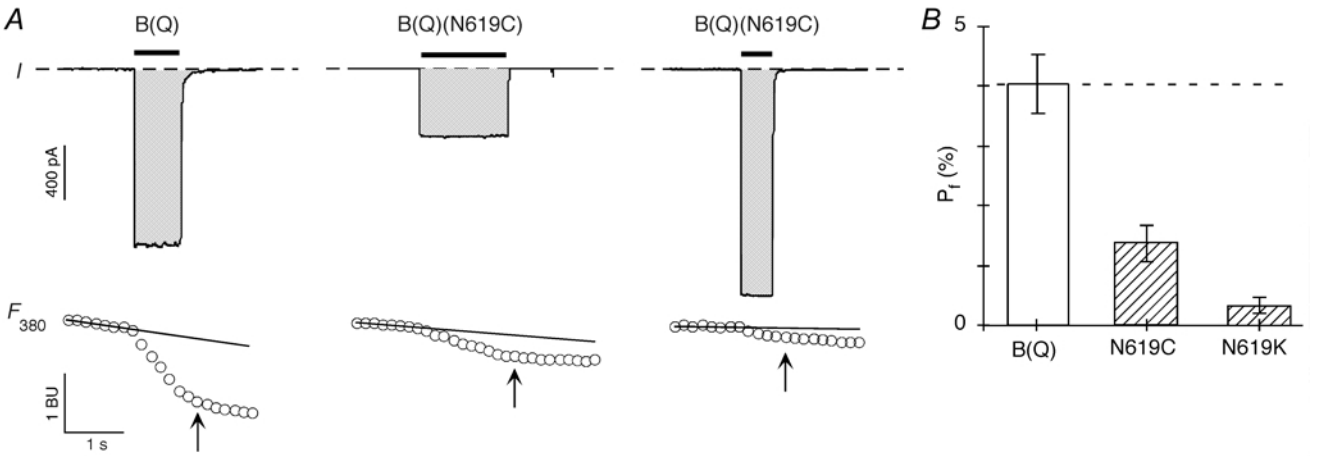


**Figure 3. Effect of substitutions of the conserved N in GluR-B(Q) channels on fractional $Ca^{2+}$ currents**

*A*, simultaneous measurement of whole-cell currents (*I*; upper panels) and fluorescence intensity with 380 nm excitation ($F_{380}$; lower panels) evoked by glutamate applications (horizontal bars) in HEK 293 cells expressing wild type GluR-B(Q) (left panel), GluR-B(Q)(N619C) (middle panel) or GluR-B(Q)(N619K) (right panel) subunits. The potential ($V$) was −60 mV to the reversal potential (see Methods). In the current records (upper panels), the dashed lines represent '0' current, and the shaded regions correspond to the current integral ($Q_T$), which was approximately the same for each of the example records. The $F_{380}$ plot is expressed in bead units (BU). We derived $\Delta F_{380}$ as the difference between the $F_{380}$ amplitude at the indicated time (arrow) and the baseline $F_{380}$ signal (horizontal line), extrapolated from a linear fit to the $F_{380}$ amplitudes prior to the glutamate application. Cells were bathed in 1.8 mM $CaCl_2$ and 140 mM NaCl. *B*, mean $P_f$ values measured at −60 mV relative to the reversal potential. The dashed line represents the average $P_f$ value for GluR-B(Q) channels. It also approximately represents the predicted $P_f$ for a channel that is cation non-selective, that is $P_{Na}/P_K = 1 = P_{Ca}/P_{Na}$ (see Jatzke *et al.* 2002). From left to right $n$ = 6, 6 and 5.

A polar threonine (T) residue is present in the highly conserved SYTANLAAF motif and is exposed to the water interface in the NMDAR NR1 subunit (Beck *et al.* 1999). GluR-B(Q) channels containing an alanine (A) but not a lysine (K) substitution of this position were functional (data not shown). Still, in these channels, B(Q)(T617A), $Ca^{2+}$ permeability measured using reversal potentials in 1.8 mM $Ca^{2+}$ (1.5 ± 0.1, $n = 4$) was comparable to that in wild type (~1.70) (for B(Q)(N619C) the comparable value was ~0.35). We did not explore this position or other polar residues in M3 further, but this result suggests that the contribution of the conserved N is specific, possibly because of its structural location relative to the central axis of the pore.

## Substitutions of the conserved N in the M3 segment alter $Ca^{2+}$ influx under physiological conditions

An alternative means to quantify $Ca^{2+}$ influx in channels with both a monovalent and $Ca^{2+}$ permeability is the use of dye overload to measure the fraction of the total current carried by $Ca^{2+}$ (Neher, 1995). Relative to measuring $Ca^{2+}$ permeability using reversal potentials, measuring fractional $Ca^{2+}$ currents ($P_f$) is advantageous, since it directly quantifies $Ca^{2+}$ influx under physiological conditions, is model independent and can be used to characterize $Ca^{2+}$ influx over a wide voltage range.

Figure 3*A* illustrates the dye overload approach to measuring the fraction of the total current carried by $Ca^{2+}$. The upper panel shows whole-cell glutamate activated currents in HEK 293 cells expressing, from left to right, GluR-B(Q), B(Q)(N619C) or B(Q)(N619K). In all examples, the external solution contained 1.8 mM $Ca^{2+}$ in 140 mM NaCl. The application of glutamate (horizontal bar) generates an inward current. It also generates a decrement in the fluorescence signal at 380 nm excitation ($F_{380}$). With dye overload, changes in the fluorescence signal ($\Delta F_{380}$) are proportional to the total $Ca^{2+}$ influx ($Q_{Ca}$), with the proportionality constant defined by $f_{max}$ according to the relationship $Q_{Ca} = I_{Ca}dt = \Delta F_{380}/f_{max}$. Fractional $Ca^{2+}$ currents were derived from the relationship $P_f$ (%) = $Q_{Ca}/Q_T \times 100$. $Q_T$, the total charge during the defined time interval, was derived from the current integral (shaded area in the current plot) and is about of equal magnitude for all three records allowing one to directly compare the $Ca^{2+}$ ($F_{380}$) signal. The magnitude of $\Delta F_{380}$ is greatly attenuated in the mutant channels compared with wild type. As summarized in Fig. 3*B*, mean $P_f$ measurements in B(Q)(N619C) (1.3 ± 0.1 %, $n = 7$) and B(Q)(N619K) (0.3 ± 0.1 %, $n = 5$) were significantly less than those in wild type (4.0 ± 0.3 %, $n = 6$) channels. A similar attenuation in $P_f$ measurements occurs in 20 mM $Ca^{2+}$ (See Fig. 4*A*). Thus, the conserved N, like that in NMDAR channels, contributes to the process of $Ca^{2+}$ influx under physiological conditions.

In summary, in mutant channels containing substitutions of the conserved N in M3, $Ca^{2+}$ permeability derived from reversal potentials is considerably less than unity and $P_f$ values are much less than those expected for a channel that is non-selective for $Ca^{2+}$ (~4 %). These results, therefore, demonstrate that the conserved N in M3 represents a critical determinant of $Ca^{2+}$ influx in $Ca^{2+}$-permeable AMPAR channels.

## The conserved N contributes to the deviation from GHK in AMPAR channels

Changes in reversal potentials and $P_f$ measurements both assay the magnitude of $Ca^{2+}$ influx. One approach to compare these values directly is to convert $P_f$ measurements to $Ca^{2+}$ permeability using GHK

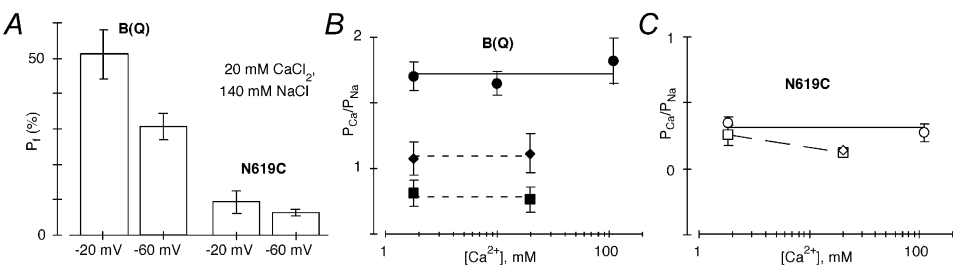


**Figure 4. Voltage and concentration dependence of $Ca^{2+}$ permeability in GluR-B(Q) and GluR-B(Q)(N619C) channels**

*A*, mean $P_f$ values measured at −20 mV (left bars) or −60 mV (right bars) in cells expressing GluR-B(Q) or B(Q)(N619C) subunits. Cells were bathed in 20 mM $CaCl_2$ and 140 mM NaCl. From left to right $n = 7$, 5, 6 and 7. *B*, comparison of $P_{Ca}/P_{Na}$ derived either from changes in reversal potential (●) or from $P_f$ measurements at −20 mM (◆) or −60 mV (■). Recordings made from GluR-B(Q) channels. The continuous line represents the average $P_{Ca}/P_{Na}$ (1.72) derived from changes in the reversal potential (Fig. 2*D*). The dashed lines show the average $P_{Ca}/P_{Na}$ derived from $P_f$ measurements in 1.8 and 20 mM $Ca^{2+}$ at −20 mV (1.1) or −60 mV (0.76). *C*, recordings made from B(Q)(N619C) channels. The continuous line shows the average $P_{Ca}/P_{Na}$ (0.31) derived from changes in the reversal potential (Fig. 2*D*). The dashed line has no theoretical meaning. Due to the reduced $Ca^{2+}$ influx and small current amplitudes, we could not reliably measure $P_f$ values at −20 mV in 1.8 mM $Ca^{2+}$ in these channels.

assumptions (e.g. Schneggenburger *et al.* 1993; Burnashev *et al.* 1995; Jatzke *et al.* 2002). We use GHK here not to test its validity for GluR channels, but rather as a reference point to compare across different experimental approaches and conditions. To convert $P_f$ values to $Ca^{2+}$ permeability, we follow the approach of Jatzke *et al.* (2002), yielding, in our ionic conditions, a $Ca^{2+}$ permeability ratio of $P_{Ca}/P_{Na}$.

Based on a comparison of the voltage and concentration dependence of $P_{Ca}/P_{Na}$ derived from changes in reversal potentials or $P_f$ measurements, AMPAR channels including GluR-B(Q) follow and deviate from GHK (see Fig. 8*B* in Jatzke *et al.* 2002). Figure 4*B* summarizes these characteristics for wild type GluR-B(Q) channels. $P_{Ca}/P_{Na}$ derived from changes in reversal potentials (filled circles) is concentration independent as are those derived from $P_f$ measurements at −20 mV (filled diamonds) or −60 mV (filled squares). Such concentration-independent $P_{Ca}/P_{Na}$ values are expected from GHK. On the other hand, while $P_f$ measurements are intrinsically voltage dependent, when this voltage dependency follows GHK, a single $P_{Ca}/P_{Na}$ will describe the values over the entire voltage range. $P_f$ measurements in AMPAR channels show much stronger voltage dependence than expected relative to GHK (Burnashev *et al.* 1995), with $P_{Ca}/P_{Na}$ derived from $P_f$ measurements getting greater in magnitude as one approaches the reversal potential (Jatzke *et al.* 2002). Accordingly, $P_{Ca}/P_{Na}$ values derived from $P_f$ values are around 0.76 at −60 mV and 1.1 at −20 mV (Fig. 4*B*). Finally, because of this voltage dependence, there is a quantitative difference between $P_{Ca}/P_{Na}$ derived from changes in reversal potentials, which is around 1.72, and that derived from $P_f$ measurements.

Figure 4*C* summarizes the voltage and concentration dependence of $P_{Ca}/P_{Na}$ in B(Q)(N619C) channels. As in wild type, $P_{Ca}/P_{Na}$ derived from reversal potentials (open circles) was concentration independent, though $P_{Ca}/P_{Na}$ derived from $P_f$ measurements at −60 mV (open squares) did show a weak concentration dependence. More distinctive relative to wild type was that $P_{Ca}/P_{Na}$ derived from $P_f$ measurements at −60 and in 1.8 mM $Ca^{2+}$ (0.26 ± 0.03) was comparable to $P_{Ca}/P_{Na}$ derived from changes in reversal potentials (~0.31). In addition, $P_{Ca}/P_{Na}$ derived from $P_f$ measurements in 20 mM $Ca^{2+}$ at − 20 mV (0.14 ± 0.02) was not significantly different from $P_{Ca}/P_{Na}$ derived at −60 mV (0.12 ± 0.02). Thus, the conserved N in M3 contributes to the pore properties that underlie the deviation from GHK in AMPAR channels, including the strong voltage dependence of $P_{Ca}/P_{Na}$ derived from $P_f$ measurements.

## The ER element does not contribute strongly to the mechanism of $Ca^{2+}$ influx in AMPAR channels

In NMDAR channels, the highly charged DRPEER motif in NR1 strongly influences the magnitude of $Ca^{2+}$ influx under physiological conditions (Watanabe *et al.* 2002). In terms of charge, DR in DRPEER is conserved in AMPAR subunits in the form of a negatively charged glutamate (E) and a positively charged arginine (R) (see Fig. 1). To study the contribution of ER to $Ca^{2+}$ influx as well as its relationship to DR in DRPEER, we generated mutant channels in which these residues were either neutralized (Fig. 5) or replaced with oppositely charged residues (Figs 5 and 6).

Figure 5*A* and *B* shows that neutralization of either E or R alters $Ca^{2+}$ influx and in a manner expected from charge neutralization. In particular, $P_{Ca}/P_{Na}$ derived from reversal potentials in 1.8 mM $Ca^{2+}$ (Fig. 5*A*) was, relative to wild type (~1.72), either significantly decreased (0.9 ± 0.1, $n = 5$) in channels where the negative charge was neutralized, B(Q)(E627A), or significantly increased (3.0 ± 0.1, $n = 5$) in channels where the positive charge was neutralized, B(Q)(R628A). $P_{Ca}/P_{Na}$ was not significantly different from that in wild type in 110 mM $Ca^{2+}$, leading to $P_{Ca}/P_{Na}$ being strongly concentration dependent. Paralleling the $P_{Ca}/P_{Na}$ values in 1.8 mM $Ca^{2+}$, $P_f$ measurements at −60 mV and in physiological conditions were significantly decreased in B(Q)(E627A) to 2.1 ± 0.2 % ($n = 9$) or significantly increased in B(Q)(R628A) to 5.5 ± 0.3 % ($n = 8$) compared with about 4 % in wild type channels (Fig. 5*B*).

The effect of charge neutralization of ER on $Ca^{2+}$ influx is consistent with the idea that these positions, similar to DR in the NR1 NMDAR subunit (Watanabe *et al.* 2002), are positioned in the ion conduction pathway and exposed to the water interface. However, the significance of ER to the overall mechanism of $Ca^{2+}$ entry in wild type channels does not seem great, since neutralization of either charge produces about equal and opposite effects. Hence, the E-to-A mutation reduces $P_f$ values by about 1.9 % whereas the R-to-A mutation increases them by about 1.5 %, suggesting that in wild type channels these charges may simply cancel each other out. Consistent with this idea, in a double-mutant channel where both charged residues were inverted (GluR-B(Q)(E627R/R628E)), $Ca^{2+}$ permeability measured in 1.8 mM $Ca^{2+}$ was indistinguishable ($P_{Ca}/P_{Na}$ = 1.8 ± 0.1, $n = 3$) from that in wild type (1.7 ± 0.1, $n = 7$) (data not shown). We will return to this point later, but note here that individual charge substitutions of ER are consistent with this idea that these charges simply cancel each other out (Figs 5*C* and *D* and 6).

## Opposite charge substitutions of ER in AMPAR channels

To further compare the function of ER in AMPARs to DR and DRPEER in general in NMDARs, we introduced opposite charge substitutions of E and R. The E-to-R substitution in all backgrounds except for GluR-B(N) did not yield glutamate-activated currents. The basis for this lack of functionality is unknown. Nevertheless, in terms of comparing ER to DR, a key experiment is the R-to-E

substitution, which produced functional channels in all backgrounds.

Figure 5*C* summarizes $P_f$ measurements at −60 mV and in 1.8 mM $Ca^{2+}$ for mutant channels containing opposite charge substitutions of E or R in three different AMPAR backgrounds, GluR-A(Q), GluR-B(Q) and GluR-B(N). In all channels containing the R-to-E substitution, $P_f$ measurements were significantly greater than those in their respective background. In A(Q)(R624E), $P_f$ measurements were 5.3 ± 0.3 % ($n = 7$) compared with 3.6 ± 0.1 % ($n = 9$) in GluR-A(Q), whereas in B(Q)(R628E), they were 6.4 ± 0.4 % ($n = 5$) compared with about 4 % in GluR-B(Q). In GluR-B channels where the glutamine at the Q/R site is replaced by asparagine (N) GluR-B(N), $P_f$ measurements are around 5 % (5.0 ± 0.2, $n = 11$). In the double-mutant channels, B(N)(R628E), $P_f$ measurements were significantly increased to 8.3 ± 0.3 % ($n = 4$). The E-to-R substitution produced functional channels only in GluR-B(N), and in these mutant channels, B(N)(E627R), $P_f$ values were significantly reduced to 1.6 ± 0.2 % ($n = 4$).

In GluR-B(N) channels, the E-to-R substitution decreased $P_f$ measurements by about 3.4 % whereas the R-to-E substitution increased them by 3.3 %. This equal and opposite effect of these charge reversals is similar to that observed for charge neutralization in GluR-B(Q) (see Figs 2*D* and 3*B*), and supports the idea that in AMPAR channels these charges make little contribution to $Ca^{2+}$ influx under physiological conditions. To test the comparable functional significance of DR in DRPEER, we measured $P_f$ values for wild type and mutant NMDAR channels containing opposite charge substitutions of DR in the NR1 subunit (Fig. 5*D*). For wild type channels, $P_f$ values were around 13.5 % (13.5 ± 0.3 %, $n = 13$). Consistent with previous results (Watanabe *et al.* 2002), $P_f$ measurements were significantly reduced in NR1(D640R) channels to 7.0 ± 0.3 % ($n = 12$) and significantly increased in NR1(R641E) to 17.1 ± 0.8 % ($n = 12$). Nevertheless, D640R reduced $P_f$ values by about 6.4 % whereas R641E increased them by only 3.6 %, suggesting that these charges are not equivalent in NMDAR channels. Thus, DR yields a net negativity that is of importance to $Ca^{2+}$ influx in contrast to ER in AMPAR channels.

### The R-to-E substitution in AMPAR channels increases $Ca^{2+}$ influx via a different mechanism than DRPEER in NMDAR channels

In AMPAR channels, the R-to-E substitution increases $P_f$ values for all three backgrounds tested (Fig. 5*C*). Presumably this effect arises because this substitution generates a high degree of negativity, C-terminal to M3, comparable with DRPEER in NMDARs. However, the results shown in Fig. 6 indicate that, while this R-to-E substitution does increase $Ca^{2+}$ influx, it does so by a mechanism distinct from that produced by DRPEER.

Figure 6*A* and *B* shows $P_{Ca}/P_{Na}$ measured using changes in reversal potentials over a wide concentration range in AMPAR channels containing the R-to-E substitution. In both A(Q)(R624E) (Fig. 6*A*) and B(Q)(R628E) (Fig. 6*B*) channels (open circles) and in contrast to their respective wild type backgrounds (filled circles), $P_{Ca}/P_{Na}$ was strongly concentration dependent, getting significantly greater in magnitude at lower $Ca^{2+}$ concentrations. Such a pattern of $P_{Ca}/P_{Na}$ is indicative of surface charges suggesting that the

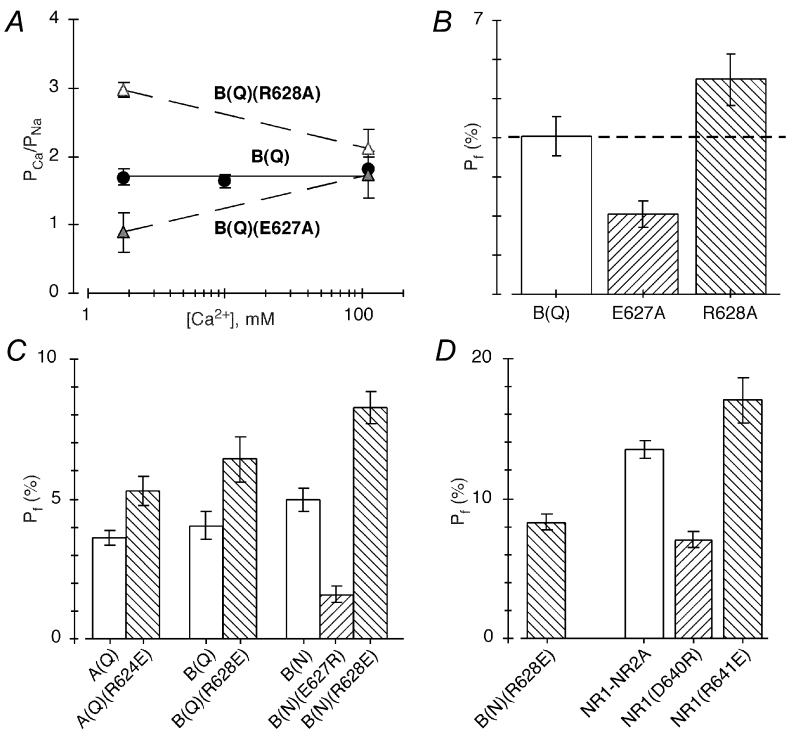


**Figure 5. The effect of substitutions of two charged residues C-terminal to M3 on $Ca^{2+}$ influx in AMPAR channels**

*A*, average $P_{Ca}/P_{Na}$ derived from changes in reversal potentials for various $Ca^{2+}$ concentrations in cells expressing GluR-B(Q), B(Q)(E627A) or B(Q)(R628A) subunits. The dashed lines have no theoretical significance. B(Q) values are the same as those shown in Fig. 2*B*. *B*, mean $P_f$ values measured at −60 mV relative to the reversal potential. Cells were bathed in 1.8 mM $CaCl_2$ and 140 mM NaCl. The dashed line represents the average $P_f$ value for GluR-B(Q) channels. *C* and *D*, mean $P_f$ values measured at −60 mV relative to the reversal potential. Cells were bathed in 1.8 mM $CaCl_2$ and 140 mM NaCl. Note the scale change in *D* with the value for B(N)(R628E) (8.3 ± 0.3 %) shown in both panels. A minimum of 4 recordings was made for each mean value.

effect of the R-to-E substitution is to increase the concentration of $Ca^{2+}$ at the surface of the channel relative to the bulk concentration. In contrast, surface charges do not contribute significantly to ion permeation in NMDAR channels (Zarei & Dani, 1994) as is illustrated by the concentration dependence of $P_{Ca}/P_{Na}$ in these channels (Wollmuth & Sakmann, 1998). To compare the overall concentration dependence of $P_{Ca}/P_{Na}$ in GluR subtypes, we normalized the $P_{Ca}/P_{Na}$ values in NMDAR channels (Fig. 6*A* and *B*, open squares) to that measured in 110 mM $Ca^{2+}$ in AMPAR channels. Like mutant AMPAR channels containing the R-to-E substitution, $P_{Ca}/P_{Na}$ increases in 110 to 1.8 mM $Ca^{2+}$. However, they diverge at 0.5 mM $Ca^{2+}$ where $P_{Ca}/P_{Na}$ continues to increase in mutant AMPAR channels but declines in NMDAR channels. Although the basis for this concentration dependence of $P_{Ca}/P_{Na}$ at low concentrations in NMDAR channels is unknown, it is associated with DRPEER (data not shown; Watanabe *et al.* 2002) and is incompatible with surface charges.

$P_{Ca}/P_{Na}$ derived from $P_f$ measurements is strongly voltage dependent in wild type AMPAR channels (e.g. Fig. 4*B*). To characterize this voltage dependence, we divided the average $P_{Ca}/P_{Na}$ derived from the $P_f$ at −20 mV by that derived at −60 mV ($(P_{Ca}/P_{Na})_{-20\,mV}/(P_{Ca}/P_{Na})_{-60\,mV}$). As shown in Fig. 6*C*, this voltage-dependent index was around 1.4 for all wild type AMPAR channels, and was not significantly changed in any of the mutant channels containing charge substitutions of ER as well as GluR-B(N) channels. On the other hand, $P_{Ca}/P_{Na}$ derived from $P_f$ measurements are voltage independent in wild type NMDAR channels, as shown by the voltage-dependent index of 1 (Fig. 6*C*). In addition, opposite charge substitutions of DR in NR1 significantly alters this voltage dependence, either increasing it (NR1(D640R)) or decreasing it (NR1(R641E)). Hence, the R-to-E substitution in AMPAR subunits, while increasing $Ca^{2+}$ influx, does not shift the voltage dependence of $P_f$ measurements towards that found in NMDAR channels. In addition, DR in NMDAR NR1 but not ER in AMPARs is positioned in the pore such that it can influence the voltage dependence of $P_f$ values. As proposed in Discussion, this difference, as well as the surface charge effect in mutant AMPAR channels, may reflect that ER in AMPARs is

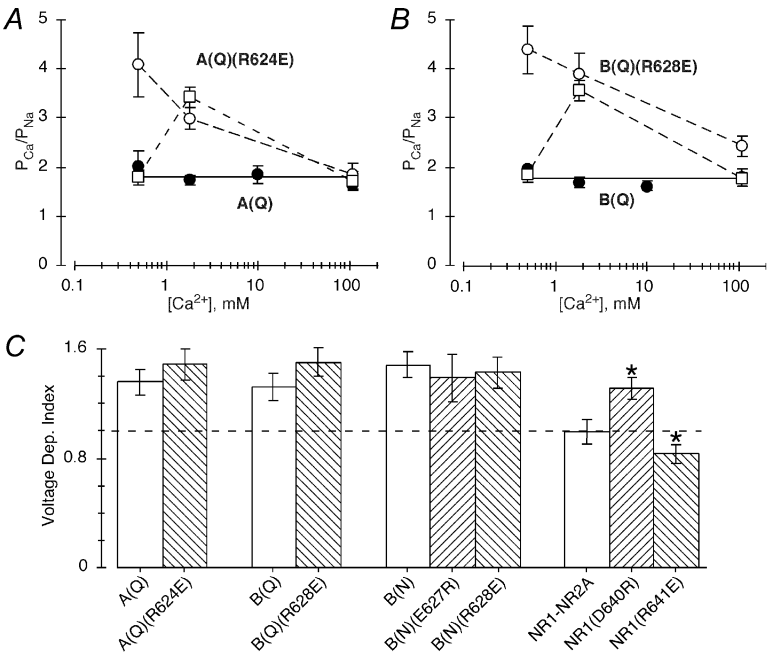


**Figure 6. Concentration and voltage dependence of $Ca^{2+}$ permeability in channels containing opposite charge substitutions**

*A*, average $P_{Ca}/P_{Na}$ derived from changes in the reversal potential for various $Ca^{2+}$ concentrations in cells expressing GluR-A(Q) (●) or A(Q)(R624E) (○) subunits. The continuous line reflects the average $P_{Ca}/P_{Na}$ (1.6) in wild type GluR-A(Q) over a concentration range of 0.5 to 110 mM $Ca^{2+}$. The dashed lines have no theoretical meaning. $P_{Ca}/P_{Na}$ for NMDAR NR1-NR2A channels normalized to the value at 110 mM $Ca^{2+}$ in wild type GluR-A(Q) channels are shown by □. The NMDAR values are from Jatzke *et al.* (2002) with the actual $P_{Ca}/P_{Na}$ values being about 3.8, 7.2 and 3.6, when measured in 0.5, 1.8 or 110 mM $Ca^{2+}$, respectively. A minimum of four recordings was made at each concentration. *B*, as in *A* except subunits are GluR-B(Q) (●) and -B(Q)(R628E) (○). *C*, voltage dependence of $Ca^{2+}$ permeability, $(P_{Ca}/P_{Na})_{-20\,mV}/(P_{Ca}/P_{Na})_{-60\,mV}$, for various wild type and mutant GluR subunit combinations. $P_{Ca}/P_{Na}$ was derived from $P_f$ values measured either at −20 or −60 mV (Table 2). The dashed line (= 1) corresponds to a channel where $P_{Ca}/P_{Na}$ shows no voltage dependence. * Values that are significantly different from those for their respective wild type channel.

positioned more externally relative to the tip of the M2 loop than DR in DRPEER in NMDAR channels.

### Negative charges C-terminal to M3 in the KAR GluR-6 subunit do not contribute to $Ca^{2+}$ permeability

C-terminal to M3 in KAR subunits, ER is present as it is in AMPAR subunits but there is an additional negative charge, specifically a glutamate (E) at position 634 (Fig. 1). Hence, KAR subunits have a potential high degree of negativity C-terminal to M3, similar to NMDAR channels, yet in contrast are poorly $Ca^{2+}$ permeable (Burnashev *et al.* 1995; Jatzke *et al.* 2002). To test the functional significance of these negative charges to $Ca^{2+}$ influx in KAR subunits, we substituted them with the oppositely charged arginine (R) (Fig. 7).

Figure 7*A–C* shows current–voltage relations for cells expressing wild type (6(Q)) or mutant GluR-6(Q) channels containing opposite charge substitutions of either position 631 (6(Q)(E631R)) or 634 (6(Q)(E634R)). In the $Na^+$ reference solution (filled circles) currents reversed in all channels near −5 mV. For wild type when $Na^+$ was replaced by $Ca^{2+}$, the reversal potential was shifted along the axis by −22.7 ± 1.0 mV ($n$ = 5) in 110 mM $Ca^{2+}$ and −75.4 ± 0.4 mV ($n$ = 6) in 1.8 mM $Ca^{2+}$. The reversal potential shifts for the mutant channels did not differ significantly from those in wild type. For 6(Q)(E631R) and

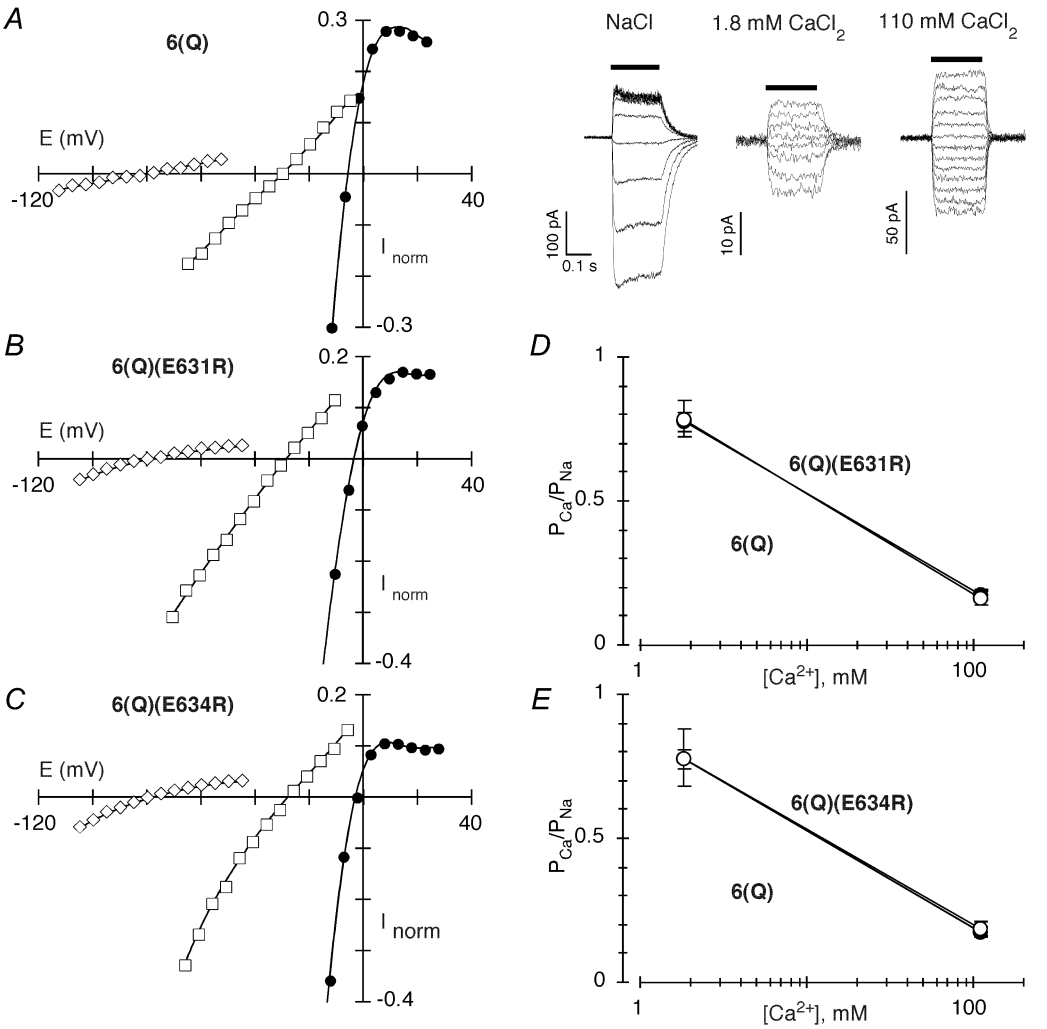


**Figure 7. The effect of opposite charge substitutions of negative charges located C-terminal to M3 in KAR subunits on $Ca^{2+}$ permeability**

*A–C*, peak glutamate-activated currents at different membrane potentials, in 2–5 mV increments, in cells expressing GluR-6(Q) (*A*), GluR-6(Q)(E631R) (*B*) or GluR-6(Q)(E634R) (*C*) subunits. Recordings were made and displayed as in Fig. 2, but because of the smaller relative current amplitudes in the $Ca^{2+}$-containing solutions, a more restricted range of the display is shown. *A*, right, corresponding whole-cell glutamate-activated currents (glutamate application, horizontal bar, 200 ms) for the GluR-6(Q) current–voltage plot shown to the left. Concanavalin A (0.3 mg $ml^{-1}$) was included in the reference solution. *D* and *E*, average $P_{Ca}/P_{Na}$ derived from changes in the reversal potential for various $Ca^{2+}$ concentrations in cells expressing wild type GluR-6(Q) (filled symbols) or 6(Q)(E631R) (*D*) or 6(Q)(E634R) (*E*) (open symbols). The lines have no theoretical meaning. A minimum of 4 recordings was made at each concentration.

6(Q)(E634R), the shifts were −25.4 ± 1.1 mV ($n$ = 5) and −23.9 ± 1.7 mV ($n$ = 4), respectively, in 110 mM $Ca^{2+}$, and −76.5 ± 0.7 mV ($n$ = 3) and −76.8 ± 1.3 mV ($n$ = 3) in 1.8 mM $Ca^{2+}$. Correspondingly, $Ca^{2+}$ permeability in channels containing these opposite charge substitutions (open circles in Fig. 7*D* and *E*), was indistinguishable from that in wild type (filled circles) at both concentrations tested. This lack of an effect of the opposite charge substitution on $P_{Ca}/P_{Na}$ is in direct contrast to what is observed for AMPAR channels even for the more subtle charge neutralization (Fig. 5*A*). Thus, these negative charges in KAR subunits do not contribute to $Ca^{2+}$ influx, presumably because they are either not exposed to the water interface or they are positioned so externally that they have no effect on ion permeation. In either case, this region in KAR channels shows a distinct structural difference from that in NMDAR and AMPAR channels.

## DISCUSSION

### Extracellular vestibule determinants of $Ca^{2+}$ influx in AMPAR channels

In GluRs, the M2 loop covers the approximate internal half of the ion pore (Kuner *et al.* 1999). The Q/R site, located at the tip of the M2 loop (Kuner *et al.* 2001), represents a key determinant of the $Ca^{2+}$ permeability properties of AMPAR channels. Although structural determinants of the extracellular vestibule in non-NMDAR channels are unknown, it is presumably formed, in homology to NMDARs, by multiple transmembrane segments including M1, M3 and M4 (Beck *et al.* 1999). Still, in NMDAR channels, the M3 segment forms the central part of the channel leading to the tip of the M2 loop (Sobolevsky *et al.* 2002*a*), and only substitutions of polar or charged residues within M3 and regions C-terminal to it alter $Ca^{2+}$ influx (Watanabe *et al.* 2002). Therefore, to identify possible determinants of $Ca^{2+}$ influx in $Ca^{2+}$-permeable AMPAR channels, we focused on M3 and regions C-terminal to it (Fig. 1). Several candidate positions were identified including polar residues in M3 and charged ones C-terminal to M3.

Our results demonstrate that a conserved asparagine (N) in M3 and specifically within the highly conserved SYTANLAAF motif contributes to the mechanism of $Ca^{2+}$ influx in $Ca^{2+}$-permeable AMPAR channels (Figs 2–4). Indeed, substitutions of this position strongly attenuated $Ca^{2+}$ permeability measured using reversal potentials and fractional $Ca^{2+}$ currents ($P_f$) measured under physiological conditions. This contribution appears specific since these same mutations do not alter polyamine block (Fig. 2*E*), suggesting that the general structure of the M2 loop including that of the Q/R site is undisturbed. Thus, in $Ca^{2+}$-permeable AMPAR channels, the process of $Ca^{2+}$ influx involves multiple sites, including (at minimum) the Q/R site and the conserved N in M3.

The M3 segment in GluRs is an important determinant of channel gating (Kohda *et al.* 2000; Sobolevsky *et al.* 2002*a*; Jones *et al.* 2002). AMPAR channels also show subconductance states (e.g. Rosenmund *et al.* 1998), some of which might have different permeation properties. Substitutions of the conserved N could therefore disrupt permeation processes indirectly, by altering the distribution of AMPAR subconductance states and/or by introducing subconductance states with different permeation properties (Schneggenburger & Ascher, 1997). Although we cannot completely rule out effects on channel gating, we believe that substitutions of the conserved N are, at minimum, directly affecting $Ca^{2+}$ permeation. First, the cysteine substitution had no apparent affect on channel gating (Table 1). Second, the magnitude of the effect was consistent with the substitution and both indices of $Ca^{2+}$ influx ($Ca^{2+}$ permeability measured using reversal potentials and $P_f$ measurements) gave the same general answer. Finally, current amplitudes were uniform and showed a single reversal potential for all mutant channels measured in the present study, in contrast to what is observed for mutant NMDAR channels which show subconductance states with different permeation properties (Schneggenburger & Ascher, 1997).

Other channels that have mixed monovalent/$Ca^{2+}$ permeability, such as NMDAR (Watanabe *et al.* 2002) and neuronal nicotinic AChR (Bertrand *et al.* 1993) channels, also contain multiple structural elements involved in $Ca^{2+}$ permeability that are distributed throughout the pore. This contrasts to voltage-gated $Ca^{2+}$ channels where the high $Ca^{2+}$ selectivity – $Ca^{2+}$ is the only permeant ion in these channels under physiological conditions – is restricted to a single locus (Ellinor *et al.* 1995). It is unknown how these different structural elements contribute to the overall process of $Ca^{2+}$ influx in channels with mixed monovalent/$Ca^{2+}$ permeability. Nevertheless, in GluR-B(Q) channels containing substitutions of the conserved N, $Ca^{2+}$ permeability derived from either reversal potentials (Fig. 2) or $P_f$ measurements (Figs 3 and 4) is significantly less than unity. Hence, these channels now select against $Ca^{2+}$ relative to monovalent ions, suggesting that simple models where a single permeation barrier defines all features of monovalent and $Ca^{2+}$ selectivity may be inappropriate.

### Deviation of $Ca^{2+}$ permeability from GHK in AMPAR channels is mediated by the extracellular vestibule

$P_f$ values are inherently voltage dependent. However, if this voltage dependence follows GHK, then a single $P_{Ca}/P_{Na}$ will describe the $P_f$ values over the entire voltage range. $P_f$ values in AMPAR channels show a much stronger voltage dependence than expected relative to GHK (Burnashev *et al.* 1995), with $P_{Ca}/P_{Na}$ derived from $P_f$ values getting

**Table 2. Fractional $Ca^{2+}$ currents ($P_f$) and $P_{Ca}/P_{Na}$ derived from $P_f$ measurements in wild type and mutant GluR channels**

| Subunit combination | $V$ (mV) | $P_f$ (%) | $P_{Ca}/P_{Na}$ | $n$ | $\Delta P_f$ |
|---|---|---|---|---|---|
| GluR-A(Q) | −20 | 6.2 ± 0.5 | 0.95 ± 0.06 | 8 | |
| | −60 | 3.6 ± 0.1 | 0.70 ± 0.03 | 9 | |
| A(Q)(R624E) | −20 | 10.2 ± 0.8 | 1.62 ± 0.10 | 5 | — |
| | −60 | 5.3 ± 0.3 | 1.09 ± 0.05 | 7 | — |
| GluR-B(Q) | −20 | 6.9 ± 0.4 | 1.07 ± 0.06 | 6 | |
| | −60 | 4.0 ± 0.3 | 0.81 ± 0.05 | 6 | |
| B(Q)(R628E) | −20 | 12.2 ± 1.2 | 2.00 ± 0.07 | 5 | — |
| | −60 | 6.4 ± 0.4 | 1.33 ± 0.06 | 5 | — |
| GluR-B(N) | −20 | 9.5 ± 0.4 | 1.50 ± 0.07 | 11 | 0 |
| | −60 | 5.0 ± 0.2 | 1.01 ± 0.04 | 11 | 0 |
| B(N)(E627R) | −20 | 2.9 ± 0.3 | 0.43 ± 0.05 | 4 | −6.6 |
| | −60 | 1.6 ± 0.2 | 0.31 ± 0.04 | 4 | −3.4 |
| B(N)(R628E) | −20 | 15.1 ± 1.5 | 2.50 ± 0.13 | 4 | 5.6 |
| | −60 | 8.3 ± 0.3 | 1.75 ± 0.06 | 4 | 3.3 |
| NR1−NR2A | −20 | 17.3 ± 0.7 | 3.81 ± 0.12 | 13 | 0 |
| | −60 | 13.5 ± 0.3 | 3.84 ± 0.09 | 13 | 0 |
| NR1(D640R)-NR2A | −20 | 11.8 ± 0.6 | 2.47 ± 0.08 | 5 | −5.5 |
| | −60 | 7.0 ± 0.3 | 1.88 ± 0.05 | 12 | −6.5 |
| NR1(R641E)-NR2A | −20 | 18.9 ± 1.2 | 4.20 ± 0.13 | 6 | 1.6 |
| | −60 | 17.1 ± 0.8 | 5.06 ± 0.10 | 12 | 3.6 |

Values are shown as means ± S.E.M. The external solution contained 1.8 mM $CaCl_2$ and 140 mM NaCl. $P_f$ measurements were converted to $P_{Ca}/P_{Na}$ using GHK (see Jatzke *et al.* 2002). $\Delta P_f$ is the difference of the mean $P_f$ values between the mutant channel and its respective background and are shown only for those channels where both E (or D) and R substitutions formed functional channels.

greater in magnitude as one approaches the reversal potential (Jatzke *et al.* 2002) (see Fig. 4*B*, left panel). Due to this voltage dependence, $P_{Ca}/P_{Na}$ derived from reversal potentials and $P_f$ values in AMPAR channels show a strong quantitative difference. Many of these deviations from GHK are greatly attenuated in channels containing substitutions of the conserved N (Fig. 4*C*). On the other hand, the asparagine substitution of the Q/R site does not alter the deviation from GHK (Jatzke *et al.* 2002) nor do ER substitutions (Fig. 6*C*; Table 2). Hence, the deviations from GHK found in AMPAR channels appear to be due primarily to energetic features of the extracellular vestibule as defined by the M3 segment.

### Subtype-specific contribution of charged residues C-terminal to M3 to $Ca^{2+}$ influx

The DRPEER motif, C-terminal to M3 in the NMDAR NR1 subunit, is a key determinant of the high $Ca^{2+}$ influx mediated by these channels (Watanabe *et al.* 2002). Our results clarify how this motif contributes to the much greater $Ca^{2+}$ influx in NMDAR channels relative to non-NMDAR subtypes. In particular, of all negative charges located C-terminal to M3, only DRPEER generates a large negativity that can influence $Ca^{2+}$ influx under physiological conditions. In part, this net negativity arises because of the excess of exposed negatively charged residues. All three negative charges (D, E and E) are exposed whereas only the first positively charged arginine is exposed (Watanabe *et al.* 2002). KAR subunits also have a net negativity in this region (Fig. 1), but none of these negatively charged residues contribute to $Ca^{2+}$ influx (Fig. 7). This could reflect a local structural difference – these positions, in contrast to homologous ones in NR1, may not be exposed to the water interface – or, alternatively, there may be a more global structural difference between subunits (see below).

Although the additional negative charges in DRPEER are important to its function, even the negativity provided by D relative to R is significant. In particular, the D-to-R substitution reduces $P_f$ values by about 6.5 %, considerably more than the 3.6 % increase produced by the R-to-E substitution (Fig. 5*D*). (An analysis of the alanine substitutions of these positions (Watanabe *et al.* 2002) yields a comparable disparity.) Further, because these substitutions alter the voltage dependence of $P_f$ values, this asymmetry is even more dramatic at −20 mV (Table 2). On the other hand, in AMPAR channels containing substitutions of residues in ER, either neutralizing them or reversing the charge (Fig. 5), $Ca^{2+}$ influx was also altered relative to wild type. Nevertheless, these substitutions have about equal and opposite effects on $Ca^{2+}$ influx measured

using reversal potentials and $P_f$ measurements. In GluR-B(Q) channels, for example, the E-to-A substitution reduces $P_f$ values by about 1.9%, whereas the R-to-A substitution increases them by about 1.5% (Fig. 3*B*). Similarly, in GluR-B(N) channels, the E-to-R substitution decreases $P_f$ values by about 3.4%, whereas the R-to-E substitution increases them by 3.3% (Fig. 5*C*). In addition, because these substitutions do not alter the voltage dependence of $P_f$ values , this equal and opposite effect occurs over the entire voltage range (Table 2). Thus, ER in AMPARs, in contrast to DR in NR1, makes little or no contribution to the mechanism of $Ca^{2+}$ influx.

### Structural asymmetry between GluR subunits

The mechanism of $Ca^{2+}$ influx in $Ca^{2+}$-permeable GluR channels, including NMDAR channels, remains unknown. Clearly, the negativity provided by DRPEER is critical to the overall process as well as to the distinction between subtypes ($Ca^{2+}$-permeable AMPAR *vs.* NMDAR). However, our results suggest that an additional difference between subtypes must also exist. Consider mutant AMPAR channels containing the R-to-E substitution, including the double-mutant channels GluR-B(N)(R624E) (Fig. 5). In these channels, there is an increase in negativity C-terminal to M3, similar to DRPEER in NR1, leading to an increase in $Ca^{2+}$ influx. However, the mechanism by which this increase occurs appears to be fundamentally different from that produced by DRPEER. Specifically, in AMPAR R-to-E mutant channels, this additional negativity acts as a surface charge (Fig. 6*A* and *B*). In contrast, surface charges do not make a significant contribution to ion permeation in NMDAR channels (Zarei & Dani, 1994), as illustrated by the concentration dependence of $Ca^{2+}$ permeability in wild type NMDAR channels (Fig. 6*A* and *B*). Further, in R-to-E mutant channels, $P_{Ca}/P_{Na}$ derived from $P_f$ values remains voltage dependent rather than becoming voltage independent as in NMDAR channels (Fig. 6*C*). Finally, substitutions of DR in NMDAR but not ER in AMPAR channels alter the voltage dependence of $P_f$ values (Fig. 6*C*).

What is the structural basis for this difference between subtypes? In part it could reflect a local structural difference, that is, negative charges may be exposed in some instances (e.g. DRPEER in NR1) whereas in other subunits (e.g. KAR and NR2) they are not. However, this explanation cannot account for the results delineated above for the R-to-E mutant channels. An alternative explanation and one consistent with the above results (though not proved by them) is that there is a global structural difference between subunits. In a comparison of NMDAR subunits, we found that relative to the tip of the M2 loop the M3 segments are staggered relative to each other, with positions in the NR2C M3 located about four amino acids more externally than homologous ones in NR1 (Sobolevsky *et al.* 2002*b*). This asymmetry may account for the fact that a cluster of three negative charges C-terminal to M3 in NR2A – occupying positions homologous to DRPEER (see Fig. 1) – makes no contribution to $Ca^{2+}$ influx (Watanabe *et al.* 2002). Hence, although DRPEER is located externally, it is positioned closer to the tip of the M2 loop than homologous residues in NR2. The more external positioning of charged residues C-terminal to M3 in NR2 subunits – and presumably also in AMPAR and KAR subunits – is sufficient to remove them from significantly influencing $Ca^{2+}$ influx. Nevertheless, the overall positioning of subunits in NMDAR, AMPAR and KAR channels is unknown. Clarifying this issue will help define basic channel properties such as ion permeation and block.

## REFERENCES


Beck C, Wollmuth LP, Seeburg PH, Sakmann B & Kuner T (1999). NMDAR channel segments forming the extracellular vestibule inferred from the accessibility of substituted cysteines. *Neuron* **22**, 559–570.

Bertrand D, Galzi JL, Devillers-Thiery A, Bertrand S & Changeux JP (1993). Mutations at two distinct sites within the channel domain M2 alter calcium permeability of neuronal alpha 7 nicotinic receptor. *Proc Natl Acad Sci U S A* **90**, 6971–6975.

Bowie D & Mayer ML (1995). Inward rectification of both AMPA and kainate subtype glutamate receptors generated by polyamine-mediated ion channel block. *Neuron* **15**, 453–462.

Burnashev N (1996). Calcium permeability of glutamate-gated channels in the central nervous system. *Curr Opin Neurobiol* **6**, 311–317.

Burnashev N, Villarroel A & Sakmann B (1996). Dimensions and ion selectivity of recombinant AMPA and kainate receptor channels and their dependence on Q/R site residues. *J Physiol* **496**, 165–173.

Burnashev N, Zhou Z, Neher E & Sakmann B (1995). Fractional calcium currents through recombinant GluR channels of the NMDA, AMPA and kainate receptor subtypes. *J Physiol* **485**, 403–418.

Dingledine R, Borges K, Bowie D & Traynelis SF (1999). The glutamate receptor ion channels. *Pharmacol Rev* **51**, 7–61.

Ellinor PT, Yang J, Sather WA, Zhang JF & Tsien RW (1995). $Ca^{2+}$ channel selectivity at a single locus for high-affinity $Ca^{2+}$ interactions. *Neuron* **15**, 1121–1132.

Gu JG, Albuquerque C, Lee CJ & MacDermott AB (1996). Synaptic strengthening through activation of $Ca^{2+}$-permeable AMPA receptors. *Nature* **381**, 793–796.

Iino M, Goto K, Kakegawa W, Okado H, Sudo M, Ishiuchi S, Miwa A, Takayasu Y, Saito I, Tsuzuki K & Ozawa S (2001). Glia-synapse interaction through $Ca^{2+}$-permeable AMPA receptors in Bergmann glia. *Science* **292**, 926–929.

Jatzke C, Watanabe J & Wollmuth LP (2002). Voltage and concentration dependence of $Ca^{2+}$ permeability in recombinant glutamate receptor subtypes. *J Physiol* **538**, 25–39.

Jones KS, VanDongen HM & VanDongen AM (2002). The NMDA receptor M3 segment is a conserved transduction element coupling ligand binding to channel opening. *J Neurosci* **22**, 2044–2053.

Koh D-S, Burnashev N & Jonas P (1995). Block of native $Ca^{2+}$-permeable AMPA receptors in rat brain by intracellular polyamines generates double rectification. *J Physiol* **486**, 305–312.

Kohda K, Wang Y & Yuzaki M (2000). Mutation of a glutamate receptor motif reveals its role in gating and d2 receptor channel properties. *Nat Neurosci* **3**, 315–322.

Köhler M, Burnashev N, Sakmann B & Seeburg PH (1993). Determinants of $Ca^{2+}$permeability in both TM1 and TM2 of high-affinity kainate receptor channels: diversity by RNA editing. *Neuron* **10**, 491–500.

Kuner T, Beck C, Sakmann B & Seeburg PH (2001). Channel-lining residues of the AMPA receptor M2 segment: structural environment of the Q/R site and identification of the selectivity filter. *J Neurosci* **21**, 4162–4172.

Kuner T, Wollmuth LP & Sakmann B. (1999). The ion-conducting pore of glutamate receptor channels. In *Ionotropic Glutamate Receptors in the CNS*, ed. Jonas P & Monyer H, pp. 219–249. Springer-Verlag, Berlin.

Liu SQ & Cull-Candy SG (2000). Synaptic activity at calcium-permeable AMPA receptors induces a switch in receptor subtype. *Nature* **405**, 454–458.

Mahanty NK & Sah P (1998). Calcium-permeable AMPA receptors mediate long-term potentiation in interneurons in the amygdala. *Nature* **394**, 683–687.

Neher E (1995). The use of fura-2 for estimating Ca buffers and Ca fluxes. *Neuropharmacology* **34**, 1423–1442.

Rosenmund C, Stern-Bach Y & Stevens CF (1998). The tetrameric structure of a glutamate receptor channel. *Science* **280**, 1596–1599.

Schneggenburger R & Ascher P (1997). Coupling of permeation and gating in an NMDA-channel pore mutant. *Neuron* **18**, 167–177.

Schneggenburger R, Zhou Z, Konnerth A & Neher E (1993). Fractional contribution of calcium to the cation current through glutamate receptor channels. *Neuron* **11**, 133–143.

Seeburg PH (1993). The TINS/TiPS Lecture. The molecular biology of mammalian glutamate receptor channels. *Trends Neurosci* **16**, 359–365.

Seeburg PH, Higuchi M & Sprengel R (1998). RNA editing of brain glutamate receptor channels: mechanism and physiology. *Brain Res Brain Res Rev* **26**, 217–229.

Sobolevsky AI, Beck C & Wollmuth LP (2002*a*). Molecular rearrangements of the extracellular vestibule in NMDAR channels during gating. *Neuron* **33**, 75–85.

Sobolevsky AI, Rooney L & Wollmuth LP (2002*b*). Staggering of Subunits in NMDAR Channels. *Biophys J* **83**, 3304–3314.

Watanabe J, Beck C, Kuner T, Premkumar L & Wollmuth LP (2002). DRPEER: A motif in the extracellular vestibule conferring high $Ca^{2+}$ flux rates in NMDA receptor channels. *J Neurosci* **22**, 10209–10216.

Wollmuth LP & Sakmann B (1998). Different mechanisms of $Ca^{2+}$ transport in NMDA and $Ca^{2+}$-permeable AMPA glutamate receptor channels. *J Gen Physiol* **112**, 623–636.

Zarei MM & Dani JA (1994). Ionic permeability characteristics of the *N*-methyl-D-aspartate receptor channel. *J Gen Physiol* **103**, 231–248.

**Acknowledgements**

We thank Drs A. Sobolevsky, M. Yelshanksy and J. Watanabe for their comments on the manuscript, and L. Rooney, M. Yelshanksy, W. Raab and S. Masterson for technical assistance. M. Hernandez was a Howard Hughes Medical Institute (HHMI Grant no. 52003052) Undergraduate Summer Research Scholar. This work was supported by NIH RO1 grant NS39102 and a Sinsheimer Scholars Award (L.P.W.).

**Author's present address**

C. Jatzke: Department of Preclinical Research and Development, Merz Pharmaceuticals GmbH, Eckenheimer Landstrasse 100, 60318 Frankfurt/Main, Germany.